Article

Tracking the Land Use/Land Cover Change in an Area with Underground Mining and Reforestation via Continuous Landsat Classification

Jiaxin Mi [1], Yongjun Yang [1], Shaoliang Zhang [1],* [iD]**, Shi An [1], Huping Hou [1], Yifei Hua [2] and Fuyao Chen [1]**

[1] School of Environment Science and Spatial Informatics, China University of Mining and Technology, Xuzhou 221116, China
[2] School of Management, China University of Mining and Technology, Xuzhou 221116, China
* Correspondence: slzhang@cumt.edu.cn; Tel.: +86-0516-8359-1301

check for updates

Abstract: Understanding the changes in a land use/land cover (LULC) is important for environmental assessment and land management. However, tracking the dynamic of LULC has proved difficult, especially in large-scale underground mining areas with extensive LULC heterogeneity and a history of multiple disturbances. Additional research related to the methods in this field is still needed. In this study, we tracked the LULC change in the Nanjiao mining area, Shanxi Province, China between 1987 and 2017 via random forest classifier and continuous Landsat imagery, where years of underground mining and reforestation projects have occurred. We applied a Savitzky–Golay filter and a normalized difference vegetation index (NDVI)-based approach to detect the temporal and spatial change, respectively. The accuracy assessment shows that the random forest classifier has a good performance in this heterogeneous area, with an accuracy ranging from 81.92% to 86.6%, which is also higher than that via support vector machine (SVM), neural network (NN), and maximum likelihood (ML) algorithm. LULC classification results reveal that cultivated forest in the mining area increased significantly after 2004, while the spatial extent of natural forest, buildings, and farmland decreased significantly after 2007. The areas where vegetation was significantly reduced were mainly because of the transformation from natural forest and shrubs into grasslands and bare lands, respectively, whereas the areas with an obvious increase in NDVI were mainly because of the conversion from grasslands and buildings into cultivated forest, especially when villages were abandoned after mining subsidence. A partial correlation analysis demonstrated that the extent of LULC change was significantly related to coal production and reforestation, which indicated the effects of underground mining and reforestation projects on LULC changes. This study suggests that continuous Landsat classification via random forest classifier could be effective in monitoring the long-term dynamics of LULC changes, and provide crucial information and data for the understanding of the driving forces of LULC change, environmental impact assessment, and ecological protection planning in large-scale mining areas.

Keywords: LULC change; underground mining and reforestation; random forest classifier; heterogeneous area; continuous Landsat classification

---

1. Introduction

The development of land use/land covers (LULC), as a manifestation of the structure and function of socio-ecological systems, reflects the transformation of regional ecosystems and socioeconomics [1–4]. In an area with extensive human activity, such as a mining area, several disturbances are likely to significantly change the LULC [5–8]. LULC of these areas are more likely to change dramatically in terms of their level of heterogeneity, based on disturbances from both continuous underground mining and restoration activities at the surface. The former usually causes loss of vegetation, destruction of buildings, and soil degradation, while the latter results in reconstruction of the modified LULC through activities such as reforestation [9–16]. Monitoring LULC changes can provide critical information related to eliminating disturbances and developing new land management plans, which will benefit both the environment and the management of a mining area [17–19]. Because LULC changes occur at large spatial and temporal scales, traditional field surveys, such as geodetic surveys and cadastral surveys, have proven to be inadequate for documenting dynamic and long-term changes to LULC due to the high costs of fieldwork.

Remote sensing provides an effective approach to monitoring the LULC changes in mining areas. In comparison with traditional field surveys, remote sensing can help researchers track long-term changes of the LULC at a low cost. Previous studies have applied remote sensing to monitor the LULC in numerous mining areas. The changes in LULC of the Tortiya mining area within 46 years were detected by supervised classification via Corona and Landsat images [20]; the surface mines within the United States were classified to revealed the changes between 2001 and 2006 [21]; the distribution of land use/land covers in mining areas was also mapped by classification via multiple remote sensing imagery [22,23]. In these studies, supervised classification is the most important approach to obtaining the LULC data, such as using random forest, a support vector machine, as well as the maximum likelihood and neural network methods [24–26]. As for remote sensing imagery with medium resolution, like Landsat images, it could be hard to identify and classify the LULC directly. To address this, field investigation and extra data such as elevation information and normalized difference vegetation index (NDVI), were adopted frequently to improve classification precision [27].

The detection of the dynamics of a LULC can prove to be difficult, especially in highly heterogeneous mining areas with multi-factor disturbances [28]. Traditionally, changes in the LULC have been demonstrated via multiple or two-date comparisons of LULC units, which could show spatial and temporal changes between two years and simulate the entire trend of LULC changes [29–31]. Some existing LULC products were also produced to richen the understanding of LULC changes, such as the Fine Resolution Observation and Monitoring of Global Land Cover (FROM-GLC) map and the 30-m resolution Global Land Cover Dataset (GLOBELAND) [32,33]. However, these dynamics may be inadequate to understand the effect of surface activities on the LULC due to discontinuous and scarce classification results, which would be particularly significant in an area with a variety of disturbance types. Frequent and remarkable LULC changes have often occurred in these areas, showing little regular pattern of change. To overcome these gaps, some researchers have also proposed the use of consecutive monitoring methods, such as a LandTrendr algorithm [34]. This type of algorithm tracks a single spectral value or vegetation index in each cell of all available remote sensing images in a study area to represent localized LULC change [35,36]. This approach, however, can only be applied in an area with single LULC type, because different LULC are difficult to differentiate when diverse objects might show the same value or index [37]. Overall, the effect of multi-factor disturbances on LULC are still not well understood, and a method that can be used to acquire continuous and long-term LULC change data in an area with strong heterogeneity and multi-factor disturbances is still lacking.

This research aimed to monitor LULC change in a mining area with a strong heterogeneity and multi-factor disturbances via continuous Landsat classification. We adopted a random forest classifier and selected the Nanjiao Mining Area, Datong City, Shanxi Province as the study area, where local features include continuous mining activities and reforestation, as well as diverse LULC. In the Nanjiao mining area, the generally low vegetation cover is mainly composed of cold- and drought-tolerant

coniferous forests, shrubs, and some herbaceous vegetation. A long history of coal mining in the Nanjiao mining area can be traced back 1500 years. By the end of 2000, 191 coal mining enterprises were active in the southern suburbs [38]. After the coal mine consolidation efforts were completed in 2010, a total of 43 coal mines were retained having a total production capacity of 57.08 million tons annually. Between 1949 and 2003, the cumulative coal mine output reached 113.2 million in total. The large-scale mining of coal has led to a large area of subsidence which, as of 2015, involved 331.59 km^2. Therefore, a series of ecological restoration projects have been carried out in the Nanjiao district.

The present study had three objectives: (1) To evaluate the performance of continuous Landsat classification via random forest classifier in revealing LULC changes in heterogeneous regions; (2) to monitor the dynamics of LULC in an area with intense mining activity and afforestation from 1987 to 2017; and (3) to discuss the effects of underground mining and afforestation projects on the LULC.

2. Materials and Methods

2.1. Study Area

The research was conducted in the Nanjiao mining area, located in Nanjiao District, Datong City, Shanxi Province, China (Figure 1). Here, the semi-arid continental climate features a mean annual temperature of 6.4°C and mean annual precipitation of 384.6 mm, with precipitation mainly occurring from June to September. The loess soil here is typically composed of approximately 64% sand (50–2000 μm), 24% silt (2–50 μm), and 12% clay (< 2 μm). The Pingchuan hills dominate the area, while the terrain elevation is generally high in the northwest and low in the southeast, with an average elevation of 1250 m. This area with coal mining subsidence covers five townships (the townships of Pingwang, Kouquan, and Ya'er Cliff, and the towns of Gaoshan and Yungang), with a total area of 459.37 km^2.
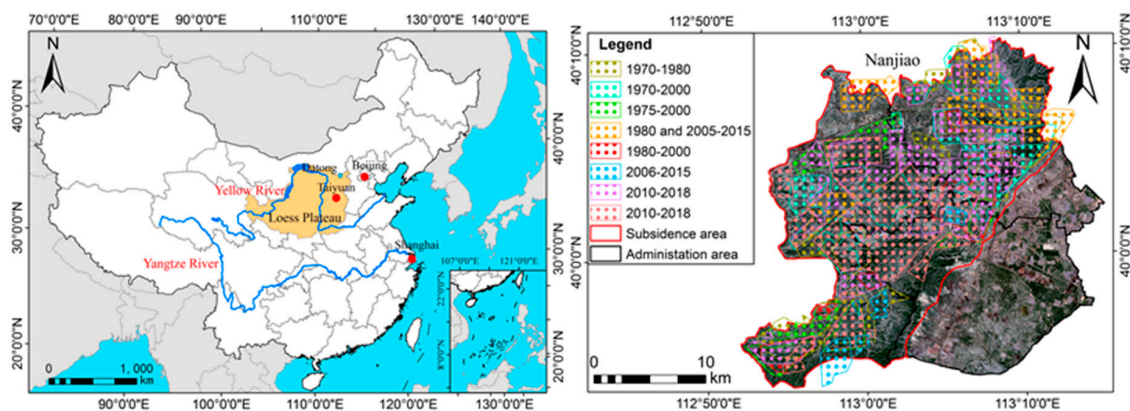

Figure 1. Location of the Nanjiao mining area and the distribution of the subsidence area. The boxes with years in legend represent the durations of mining activities occurring in each area.

In addition, to address severe wind and soil erosion in the region, China has implemented several major reforestation projects simultaneously—the most important of them being the Three-North Shelter Forest Program (since 1987) and the Beijing-Tianjin Sandstorm Source Control Project (since 2002) [39,40]. The reforestation efforts involved the cultivation of introduced vegetation, mainly trees (pine and poplar) and shrubs (sea buckthorn), which were mainly distributed in the mining area after land reclamation and abandoned farmland. The coal production and reforestation area from 1987 to 2017 in this area were collected and shown as Figure 2. All mining-related data in this study were acquired from Bureau of Land and Resources in Nanjiao district, Datong city.
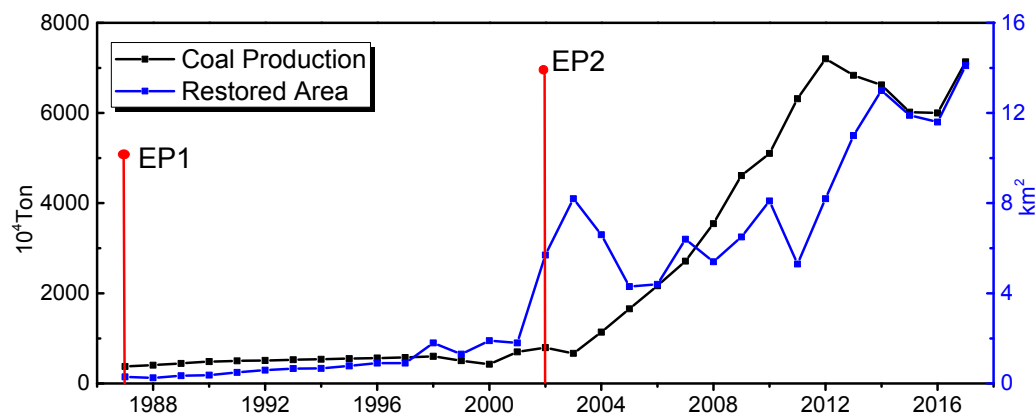
Figure 2. Coal production and reforestation from 1987 to 2017. EP1 (Ecological project 1): Three-North Shelter Forest Program. EP2 (Ecological project 2): Beijing-Tianjin Sandstorm Source Control Project.

2.2. Training Sample and Datasets

2.2.1. Training Sample Collection

High precision training samples and an appropriate classification system are the perquisite of LULC classification. In this study, we combined both imagery observation and field investigation to determine classification system and training samples. Firstly, we concluded categories of potential LULC via Landsat imagery, Google Earth images and acquired land use maps, and those which cannot be determined were marked. Then, we conducted field surveys in the Nanjiao district from 26–29 September, 2018 to verify these LULC and correct misclassified objects. For example, the forest in the study area was divided into three categories: Natural forest, cultivated forest, and mixed forest. As for natural forest, which is mainly located on the mountain with a high elevation, it was dense and dominated by pine; cultivated forest was distributed on the plain with low Digital Elevation Model (DEM) value, and mainly consisted of poplar, planted in an intensive and tidy pattern; mixed forest developed under spontaneous succession in the long term, and was made up of trees, shrubs, and grass, which was usually in a loose pattern and poor growth condition due to lack of management. They showed different spectral characteristics on Landsat images due to their species and density of tree. In the Landsat image with false-color composite, natural forest, cultivated forest, and mixed forest showed black, dark red, and dull red, respectively, as shown in Figure 3. In summary, we determined a total of ten LULC types, including natural forest, cultivated forest, mixed forest, high-coverage grassland, low-coverage grassland, shrubs, buildings, farmland, bare land, and photovoltaic panels. Among these, photovoltaic panel was a relatively novel LULC in this area which appeared in 2015, according to Landsat imagery.

Based on defended LULC, a total of 265 regions of interest (about 25 sample polygons for each LULC that included 1350 points) were selected by visual interpretation in 2017, and the distribution of these samples was shown in Figure 4a. As for the images in previous years, we took the spectral characteristic of each LULC in 2017, documented Google Earth images and acquired land use maps as references to select regions of interest in previous years, and 7655 sample polygons (more than 250 samples including about 1250 points in each year) in total were chose from 1987 to 2017. To test the difference of determined samples in spectral characteristics, and select the imagery in the suitable season participating in supervised classification, we compared the average of the pixel spectral value and the annual normalized difference vegetation index (NDVI) changes (NDVI in 2016 was chosen as an example) in each sample respectively (Figure 4b,c). The spectral curve illustrated the deviance of selected samples for each LULC, and NDVI changes revealed that the images between 1 August and 30 September could be the best duration for classification. In addition, the NDVI values of each LULC were ascertained with the reference of the annual NDVI change in previous years, which were obtained from the dataset on Google Earth Engine, including Landsat 8 32-Day NDVI Composite,

Landsat 7 32-Day NDVI Composite, and Landsat 5 32-Day NDVI Composite [41]. At last, we acquired the classification system and samples in all years, and a detailed description of determined LULC is shown in Table 1.
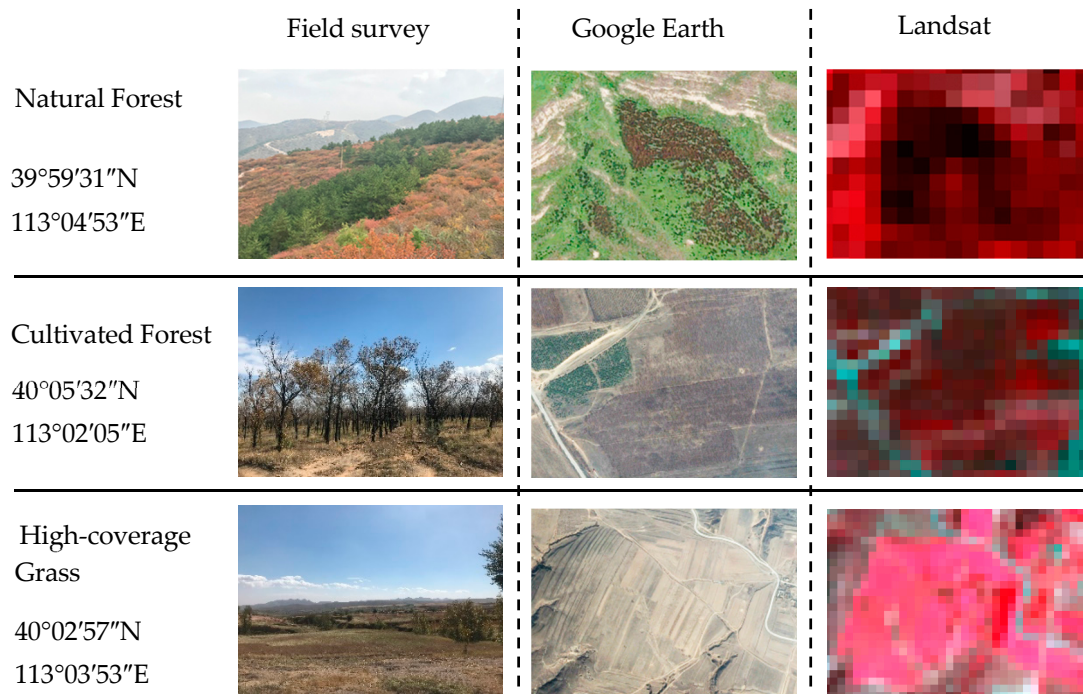
	Field survey	Google Earth	Landsat
Natural Forest 39°59′31″N 113°04′53″E			
Cultivated Forest 40°05′32″N 113°02′05″E			
High-coverage Grass 40°02′57″N 113°03′53″E			

Figure 3. A comparison of remote sensing images and field survey photos. Landsat image was composited with false-color (RGB: Band 432).

Table 1. A detailed description of each land use/land cover (LULC).

Classification Type	Standard
Natural forest	High density pine; NDVI > 0.5; black in false-color composite; high elevation
Cultivated forest	High density Poplar; NDVI > 0.5; dark red in false-color composite; low elevation
Mixed forest	Low density tree; 0.3 < NDVI < 0.5; dull red in false-color composite
High-coverage grassland	High density grass; 0.3 < NDVI < 0.5; pink in false-color composite
Low-coverage grassland	Low density grass; 0.2 < NDVI < 0.3; baby pink in false-color composite
Shrubs	High density shrubs; NDVI > 0.5; bright red in false-color composite
Farmland	Crop; NDVI > 0.5; red in false-color composite; low elevation
Buildings	Impervious surface; NDVI < 0.2
Bare land	Non-vegetation surface; NDVI < 0.2; white in false-color composite
Photovoltaic panel area	Photovoltaic panel; 0.3 < NDVI < 0.5; blackish green in false-color composite (because of the vegetation under panel); low elevation

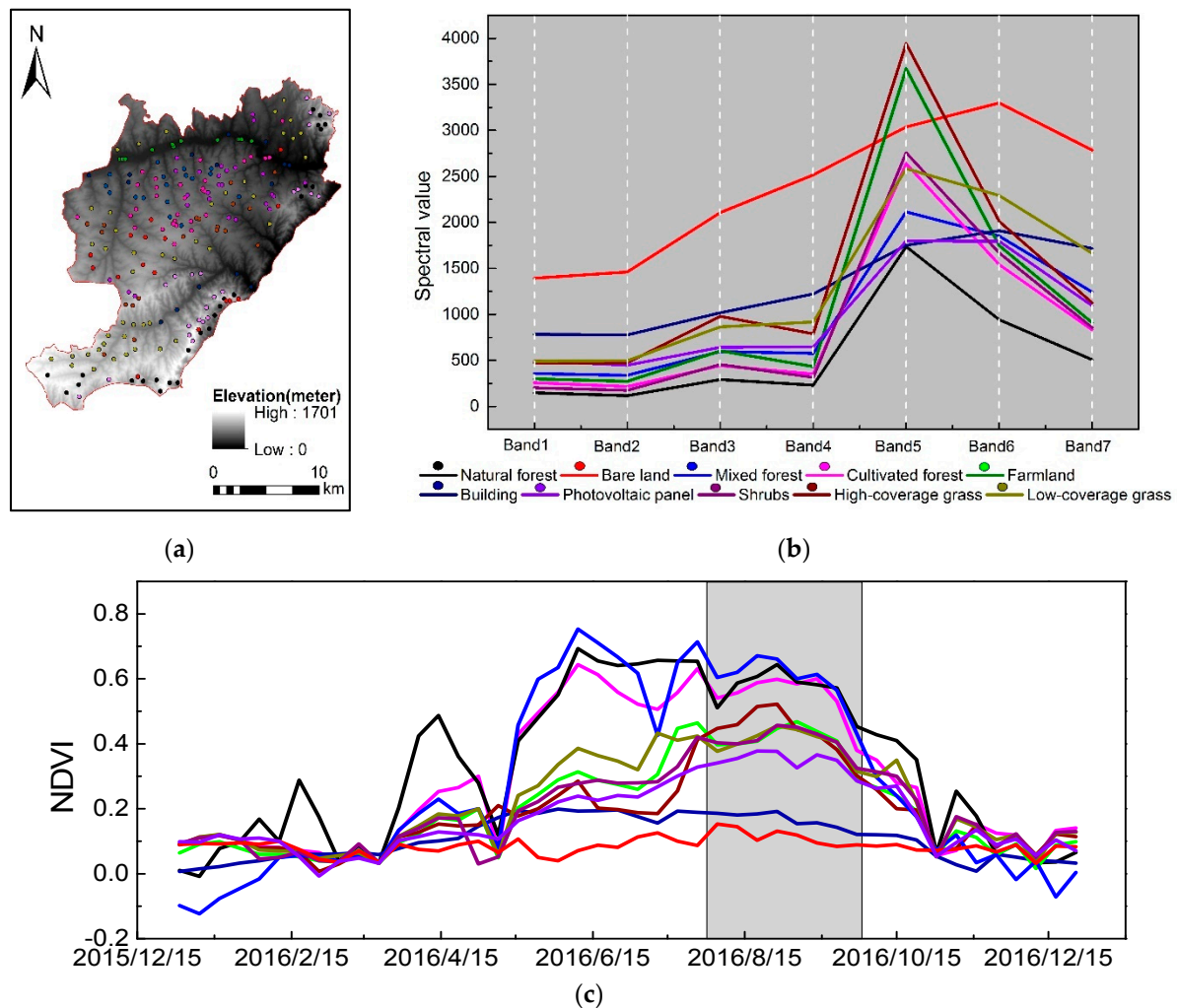**Figure 4.** Training sample information: (**a**) Distribution of training samples; (**b**) spectral characteristics of the samples; (**c**) annual changes in the normalized difference vegetation index (NDVI) of samples. Note: The grey area in (**c**) represents the duration of images selected for classification.

2.2.2. Data Preparation

Landsat4/5 thematic mapper, Landsat 7 enhanced thematic mapper (SLC-on), and Landsat 8 operational land imager data were employed as data resources in this research. Images acquired between August and September were reviewed in terms of the maturity of plants and crops in the Nanjiao district to minimize variations caused by plant phenology. After setting the maximum cloud cover at less than 10%, a total of 50 images acquired between 1987 and 2017 were obtained from the United States Geological Survey website (USGS, https://earthexplorer.usgs.gov/) (Table 2).

Table 2. Image acquisition date and its sensor. TM—Thematic Mapper; ETM—Enhanced Thematic Mapper; OLI—Operational Land Imager.

Period	Sensor	Acquisition Date		
1987–1997	TM	8 September 1987	26 September 1988	29 September 1989
		31 August 1990	02 August 1991	18 August 1991
		04 August 1992	24 September 1993	10 August 1994
		27 September 1994	30 September 1995	16 September 1996
		09 August 1997	25 August 1997	03 September 1997
1997–2007	ETM, TM	28 August 1998	06 September 1998	24 August 1999
		11 September 2000	21 August 2001	14 September 2001
		30 September 2001	01 September 2002	17 September 2002
		25 September 2002	03 August 2003	20 September 2003
		05 August 2004	22 September 2004	25 September 2005
		27 August 2006	12 September 2006	28 September 2006
		14 August 2007	15 September 2007	
2007–2017	TM, ETM, OLI	01 September 2008	20 September 2009	22 August 2010
		23 September 2010	09 August 2011	14 August 2013
		06 September 2013	01 August 2014	18 September 2014
		04 August 2015	20 August 2015	21 September 2015
		06 August 2016	23 September 2016	25 August 2017

Note: OLI, operational land imager; TM and ETM refer to Landsat thematic mapper and enhanced thematic mapper, respectively.

2.3. Methods

2.3.1. LULC Classification and Change Detection

Major components of continuous LULC classification are shown in Figure 5. Before LULC classification, we applied radiometric calibration and atmospheric correction (FLAASH) to the images that selected with less than 10% cloud, which were also cut according to the boundary of study area for accelerating classification process and increasing accuracy. After pre-processing the continuous images, we composted the Landsat spectrum, terrain information from the Global Digital Elevation Model of the Advanced Spaceborne Thermal Emission and Reflection Radiometer (ASTER GDEM) with 30 m resolution, and NDVI into one layer to provide input for the random forest classifier, which has been proven to be effective in many research studies [27,42].

To determine the classification algorithm used in this research for best accuracy performance, we produced LULC classification with random forest (RF), support vector machine (SVM), neural network (NN), and maximum likelihood (ML) algorithm to the 2017 image respectively. Figure 6 shows that the overall accuracy of the four classifiers exceeded 83%, and the random forest classification provided the highest accuracy. Therefore, we applied the random forest algorithm in the rest of LULC classification.

As for random forest algorithm, the accuracy depended on the number of trees and the number of random features used for classification. Among the features were NDVI and DEM, as they might improve classification accuracy. The OOB (out-of-bag) test was performed to determine the test set accuracy. According to trial and error, the number of trees and random vectors of 50 and 3, were considered as the best parameters for random forest classification of land cover/land use of the study area. The classification via SVM, NN, and ML algorithm were all performed in ENVI 5.3. As for SVM algorithm, Radial basis function was selected to be performed in this study, with Gamma in Kernel Function and Penalty Parameter equaling to 0.25 and 100, respectively; Pyramid levels was set as default values (0). During the classification with NN algorithm, logistic function was used for activation. Training threshold contribution, training rate, training momentum, and training Root mean square (RMS) exit criteria were determined as 0.9, 0.2, 0.9, and 0.1 after comparing the results with different values, and the number of training iterations was set as 100 for improving accuracy.

ML algorithm was performed with setting probability threshold with none and data scale factor with 255, according to the data type used in this research.
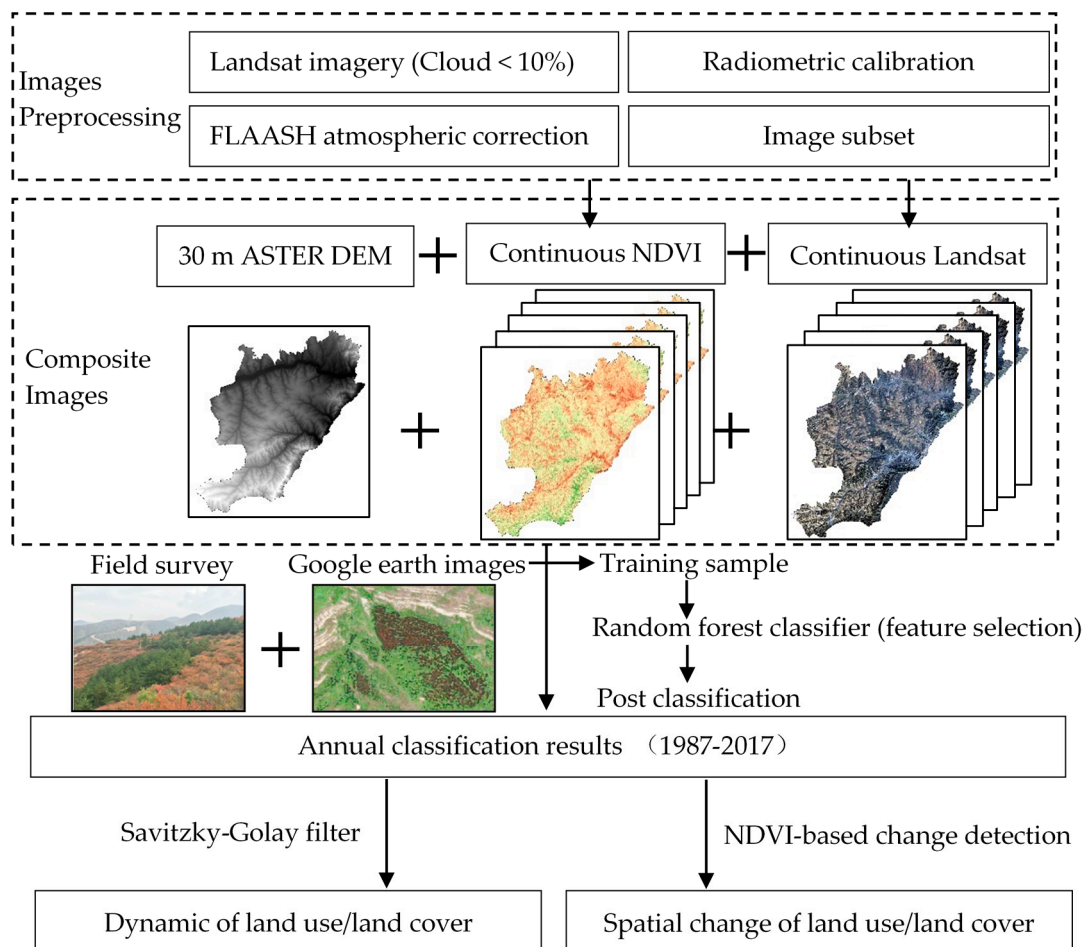

Figure 5. Workflow of the LULC classification and change detection.
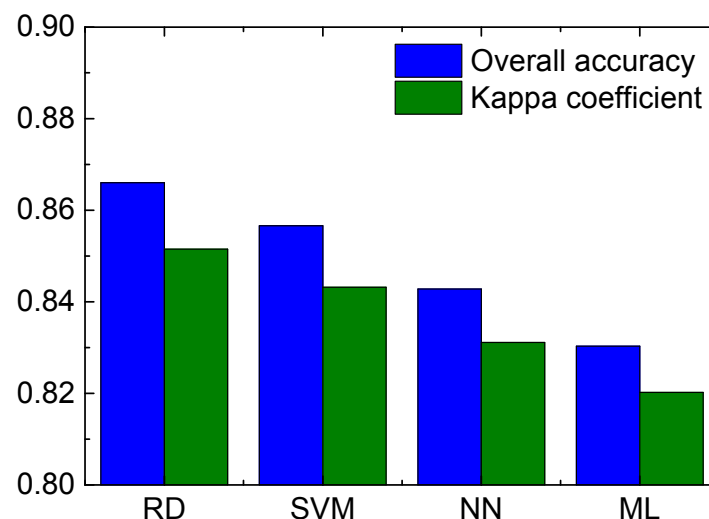

Figure 6. A comparison of the classification accuracy via four algorithms. RD: Random forest; SVM: Support vector machine; NN: Neural network; ML: Maximum likelihood.

As for the years with multiple images, we performed random forest classification for all these images respectively. The difference in LULC between classification results were selected, and the LULC

with maximum number of occurrences after comparing all results were determined as the final one. For example, if one area was classified into cropland twice and grassland one time, based on three images in one year, then cropland was determined as its LULC. At last, we combined and modified those area which have deviance among classification results via post classification in ENVI 5.3, and a composite image as the annual land use/land cover was derived in this year.

Temporal and spatial changes from 1987 to 2017 were analyzed in this research annually. After acquiring a relatively continuous set of dynamic LULC images, we applied Savitzky-Golay filter to eliminate the noise from remote sensing classifications between years, which was frequently applied to simulating the data trend in the long term [43,44].

As for spatial changes, we introduced an NDVI-based approach to detect the LULC change where the NDVI varied dramatically. Previous studies frequently adopted confusion matrix to reflect the changes of every pixel [45], and some complex detection algorithms [46,47]; however, these approaches seldom categorize the changes with different degrees of change. Underground mining and reforestation, the two main driving forces that we considered in this research, were more likely to result in greater changes in NDVI than other natural factors (climate changes and vegetation succession); such as the significant increase in NDVI when bare land was planted with trees. Thus, we applied a difference-NDVI (DNDVI) to highlight the spatial changes in LULC, especially as these might be caused by underground mining and reforestation. The equations are as shown below:

$$NDVI = (Nir - Red)/(Nir + Red) \tag{1}$$

$$DNDVI = NDVI_{t2} - NDVI_{t1} \tag{2}$$

where Nir and Red represent reflectance derived from spectral radiances, measured by the near-infrared channel and the red channel, respectively, while $NDVI_{t2}$ and $NDVI_{t1}$ are the NDVI in t2 and t1 year.

To categorize the degree of LULC change in terms of NDVI, we tried different thresholds to divide the DNDVI, and we found that the NDVI changes would effectively match the LULC changes when DNDVI equals 0.4. Thus, we divided DNDVI into five grades: Dramatic increase (DNDVI >0.4), small increase (0.1 < DNDVI < 0.4), stable (−0.1 < DNDVI < 0.1), small decline (−0.4 < DNDVI < −0.1), and dramatic decline (DNDVI < −0.4). In this research, we selected 1987 and 2017 images as examples to show the spatial changes over 30 years.

2.3.2. Accuracy Assessment

We applied a stratified random sampling strategy to test the accuracy of the classification results in the present study. In total, 30,000 points were randomly produced via ArcGIS 10.3 (ESRI, Redlands, CA, USA) within the study area, with 1000 points in each year. To make sure every class included enough sample points, we counted the number of sample points in each class and supplemented the amount by more than 100. We compared each sample to polygon attributes, field records, and Google Earth images, and identified the associated LULC categories. In addition, we also collected some existing land use/land cover products, such as the 30-m resolution Global Land Cover Dataset (GLOBELAND 30; 2000 and 2010) and the Fine Resolution Observation and Monitoring of Global Land Cover (FROM-GLC) map, which have the same spatial resolution as our classification results, to test the accuracy of our results. A confusion matrix was applied in the present study to check the accuracy of the results, because confusion matrices have been widely used in accuracy assessment. The overall accuracy and Kappa concordance coefficient of agreements (Kappa coefficient) in each year were calculated, and finally the overall accuracy of all classification results was obtained average value. The equation of Kappa coefficient is showed as below [46].

$$Kappa = \frac{N \sum_{i=1}^{r} x_{ii} - \sum_{i=1}^{r} (x_{i+} * x_{+i})}{N^2 - \sum_{i=1}^{r} (x_{i+} * x_{+i})} \tag{3}$$

where r is the number of rows in the matrix; x_{ii} is the number of pixels in row i and column i; x_{i+} and x_{+i} are the marginal totals of row i and column i, respectively; and N is the total number of pixels.

2.3.3. Data Analysis

Because the LULC in the study area was influenced by both underground mining and reforestation projects, partial correlation method was applied to describe the relationship between LULC, coal production, and reforestation area, and the partial correlation coefficient was tested via t-test at the significance level of 0.05. The partial correlation coefficients were calculated as follows:

$$\mathrm{r}_{L_i C \cdot R} = \frac{r_{L_i C} - r_{L_i R} \times r_{CR}}{\sqrt{\left(1 - r_{L_i R}^2\right) \times \left(1 - r_{CR}^2\right)}} \tag{4}$$

$$\mathrm{r}_{L_i R \cdot C} = \frac{r_{L_i R} - r_{L_i C} \times r_{CR}}{\sqrt{\left(1 - r_{L_i C}^2\right) \times \left(1 - r_{CR}^2\right)}} \tag{5}$$

where i is the number of LULC, and $\mathrm{r}_{L_i C \cdot R}$ and $\mathrm{r}_{L_i R \cdot C}$ represent the partial correlation coefficient of i_{th} LULC and coal production, and reforestation area, respectively. $r_{L_i C}$, $r_{L_i R}$, and r_{CR} were the correlation coefficients between i_{th} LULC and coal production, reforestation area, as well as between coal production and reforestation area, respectively. Curve fittings (both linear and non-linear functions) were also used to simulate the change of LULC under the effect of underground mining and reforestation projects. Software, including SPSS 19.0 and Excel, were used to perform all of the statistical analyses, with the Origin 9.0 software used for producing figures.

3. Results

3.1. Performance Assessment of the Classification

Overall accuracy and Kappa coefficient were calculated and are displayed in Table 3. The overall accuracy of classifications all exceeded 80%, ranging from 81.92% to 86.6%. In addition, the Kappa coefficients varied between 0.80 and 0.85. In general, average overall accuracy and Kappa coefficient were 84.01% and 0.82, respectively. In the years with low accuracy, some land use which had similar spectra were classified incorrectly, such as mostly occurred when low-coverage grassland and mixed forest were misclassified (see Table S1).

Table 3. Overall accuracies and Kappa coefficients of the classification results.

Years	Overall Accuracy in Each Year (%)	Kappa Coefficient	Years	Overall Accuracy in Each Year (%)	Kappa Coefficient
1987	82.4	0.81	2002	82.85	0.81
1988	83.85	0.82	2003	82.21	0.80
1989	82.46	0.81	2004	82.63	0.81
1990	84.47	0.83	2005	83.46	0.82
1991	85.6	0.84	2006	85.98	0.85
1992	83.44	0.82	2007	82.86	0.81
1993	84.8	0.83	2008	83.18	0.81
1994	84.1	0.82	2009	85.48	0.84
1995	85.92	0.84	2010	83.72	0.82
1996	81.92	0.80	2011	84.31	0.83
1997	82.81	0.81	2013	83.68	0.82
1998	83.32	0.82	2014	84.92	0.83
1999	85.91	0.84	2015	85.5	0.84
2000	82.29	0.81	2016	85.83	0.84
2001	83.78	0.82	2017	86.6	0.85
Average overall accuracy (%)				84.01	
Average Kappa coefficient				0.82	

Figure 7 compares the accuracy of random forest classification results with that of FROM-GLC and GLOBELAND 30 products. We selected a small area of the classification in 2010 as a sample. Compared with the original Landsat image (Figure 7a), the classification by random forests (Figure 7b) has a better performance in the details of land use, while FROM-GLC (Figure 7c) and GLOBELAND 30 (Figure 7d) products provide less detailed information. Some land uses were combined or ignored in the latter two classification systems, especially those that have a relatively small scale, such as buildings, shrubs, or cultivated forest. In addition, we compared the overall accuracy of the three types of classification results listed above. The overall accuracy of random forest ranked the first in its average value among these three products. It is followed by that of FROM-GLC and GLOBELAND30, with only 68.67% and 54.98%, respectively.
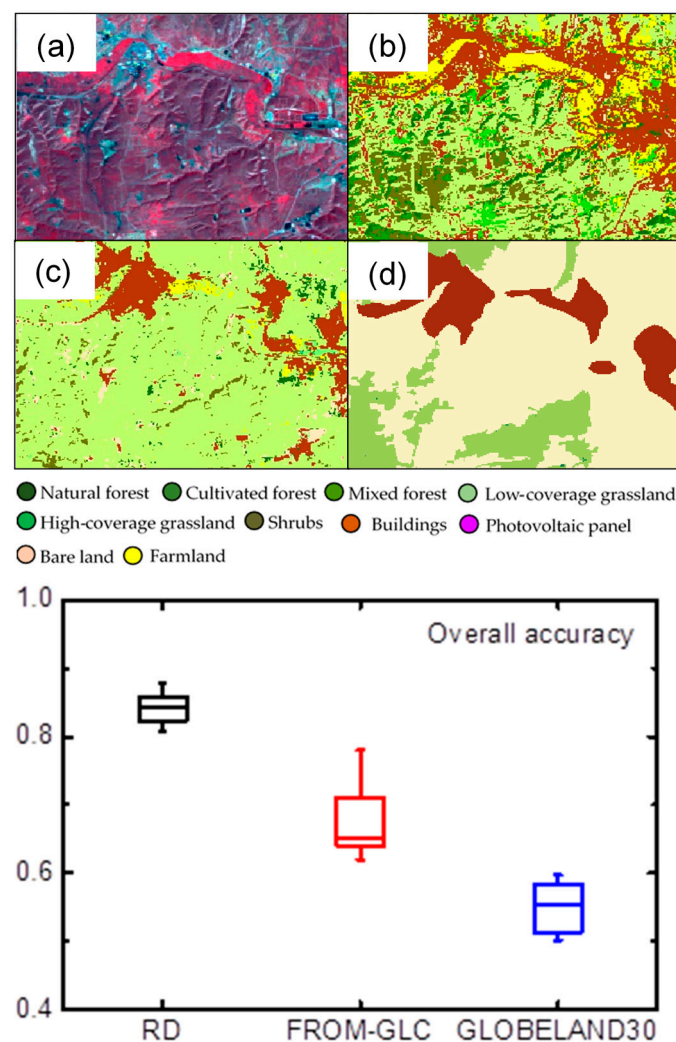

Figure 7. A comparison of the overall accuracies using Random forest classification, the Fine Resolution Observation and Monitoring of Global Land Cover (FROM-GLC) map, and the 30-m resolution Global Land Cover Dataset (GLOBELAND 30). (**a**) Landsat image with false-color composite; (**b**) Random forest classification; (**c**) FROM-GLC; and (**d**) GLOBELAND 30.

3.2. Temporal and Spatial Changes of LULC

Visualizations of LULC in the Nanjiao mining area between 1979 and 2017 are shown in Figure 8, listing detailed LULC in 1987, 1997, 2007, and 2017 as reference data (Table 4). Spatial changes obviously occurred in the northern part of the study area, where many photovoltaic panels and buildings have been constructed over the last 30 years. Meanwhile, in the mountainous area located in the southern

part of the area, the spatial extent of natural forest has decreased. As the statistical analysis shows, in 1987 the LULC was dominated by low-coverage grassland and mixed-forest land, while little farmland and cultivated forest was found in the Nanjiao mining area. After 10 years, low-coverage grassland continued to dominate in LULC pattern, while the number of buildings increased dramatically and became the second most important LULC feature. At the same time, farmland and cultivated forest continued to decline in spatial extent. Between 1997 and 2007, most LULC had experienced an increase, except for the spatial extent of areas with buildings, low-coverage grassland, and shrubs. In this period, mixed forest became the major LULC in this area. In 2017, a novel LULC, photovoltaic land, emerged in the mining area. The low-coverage grassland and mixed forest land were still the main LULC types of the region, and the extent of cultivated forest land increased significantly, while the coverage area covered by buildings declined relative to other LULC. Overall, lands with natural forest and shrubs are mainly concentrated in the mountainous areas outside the subsidence area in the southern part of the study area; the remaining LULC, such as cultivated forest land and newly-built photovoltaic panels, are within the subsidence area, and the farmland is mainly distributed around towns.
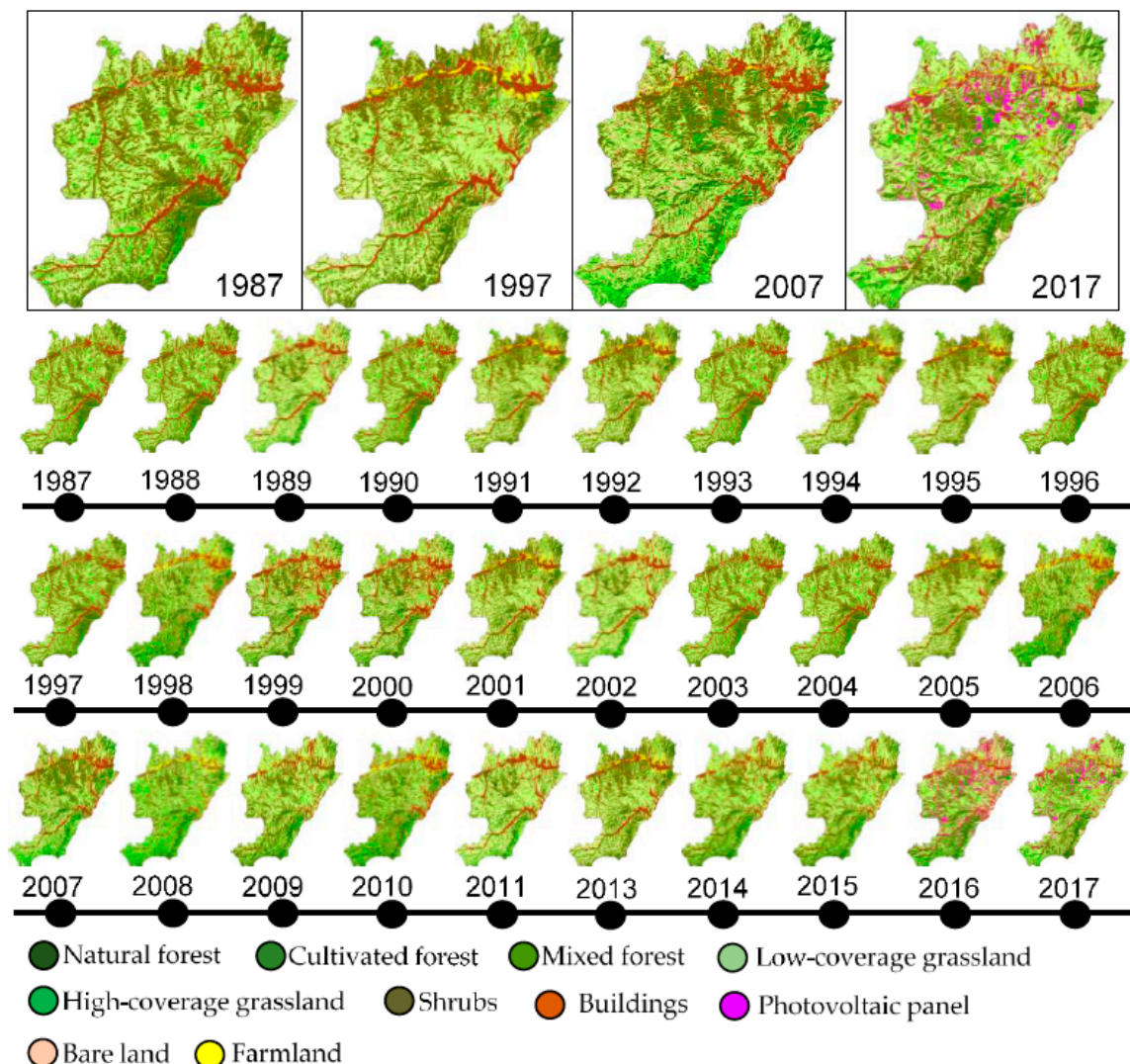
Figure 8. Continuous LULC classification between 1987 and 2017.

Figure 9 illustrates the dynamics of land use changes in the Nanjiao mining area between 1987 and 2017. The results show that the cultivated forest land (**a**) and shrubs (**d**) experienced a small fluctuation in the first 20 years, before arising dramatically since around 2005. The area of natural

forest (**b**) and farmland (**g**) kept a steady increase until about 1997, and after a significant growth, they descended since 2007 and 2004, respectively. The amount of buildings (**h**) in the study area expanded during the first 15 years and continued to expand over the following period. High-coverage grassland (**e**) remained steady in the first 15 years, and decreased significantly after 2007 following a short-lived increase, while low-coverage grassland (**f**) and bare land (**i**) showed a nearly opposite trend. The area of mixed forest land (**c**) has maintained a declining trend, except for a transient increase from 2002 to 2007.

Table 4. The LULC in 1987, 1997, 2007, and 2017. Note: HC and LC represent high-coverage and low-coverage, respectively.

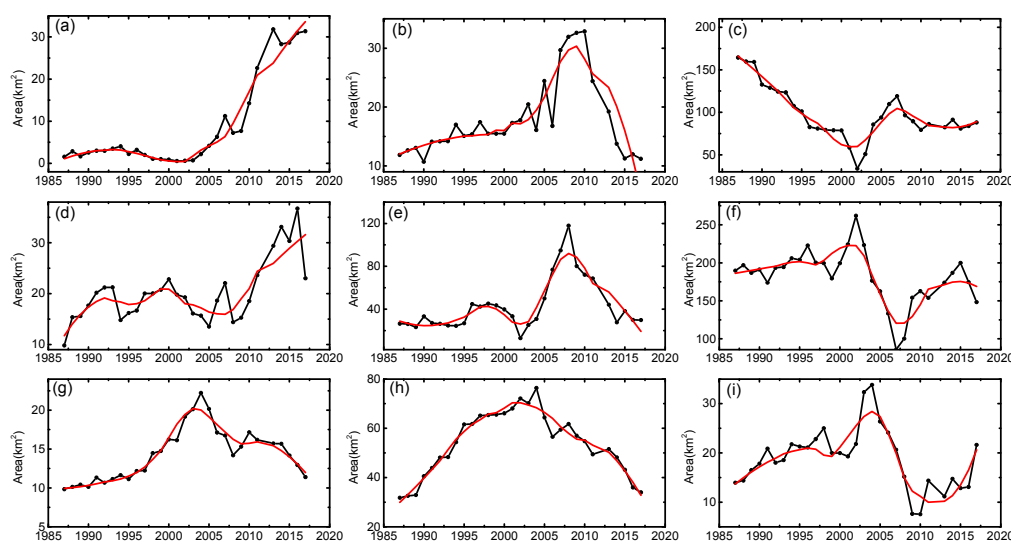| LULC\Year	1987 (km²)	1997 (km²)	2007 (km²)	2017 (km²)
Cultivated forest	1.55	0.89	11.19	31.36
Natural forest	11.87	15.49	29.67	11.21
Buildings	41.79	86.09	79.44	33.96
Farmland	0.65	0.36	16.74	11.40
HC grassland	25.62	35.61	74.78	29.80
Shrubs	9.81	22.80	22.06	23.02
Mixed forest	164.37	78.63	118.98	88.06
LC grassland	189.75	199.52	85.86	148.34
Bare land	13.96	19.98	20.65	21.64
Photovoltaic panel area	-	-	-	60.58

Figure 9. Land use changes in the mining area from 1987 to 2017. Black line: The trend line of the actual area of the land use. Red line: The trend line after Savitzky-Golay filter setting ten windows. (**a**) Cultivated forest; (**b**) natural forest; (**c**) mixed forest; (**d**) shrubs; (**e**) high-coverage grassland; (**f**) low-coverage grassland; (**g**) farmland; (**h**) buildings; (**i**) bare land.

The spatial changes in the land use of the Nanjiao mining area were detected in terms of NDVI in 1987, 1997, 2007, and 2017. A higher NDVI value of the area as a whole could be observed in 2017, while the lowest NDVI value of this region appeared in 1997 (Figure 10). In the first 10 years, the NDVI value of the Nanjiao mining area showed an overall downward trend; conversely, most areas presented an increase in NDVI value between 1997 and 2007. In the last ten years (from 2007 to 2017), both dramatic decline and rise in NDVI value were observed and distributed in this area (Figure 11). In summary, from the perspective of 30 years of development, most of the Nanjiao mining area has increased in NDVI value, while the areas that experience a significant decline in vegetation coverage were mainly distributed in the southern mountainous areas, where natural forest and shrubs had

thrived in 1987. In contrast, those areas experiencing a significant increase in vegetation coverage were mainly located in areas with an increasing intensity of human activity.
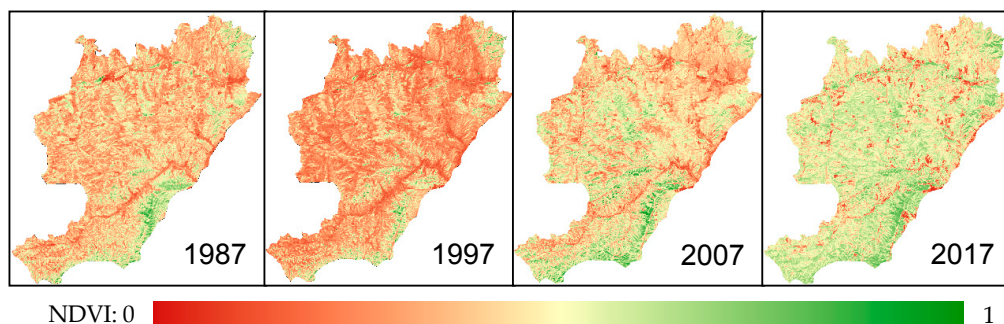

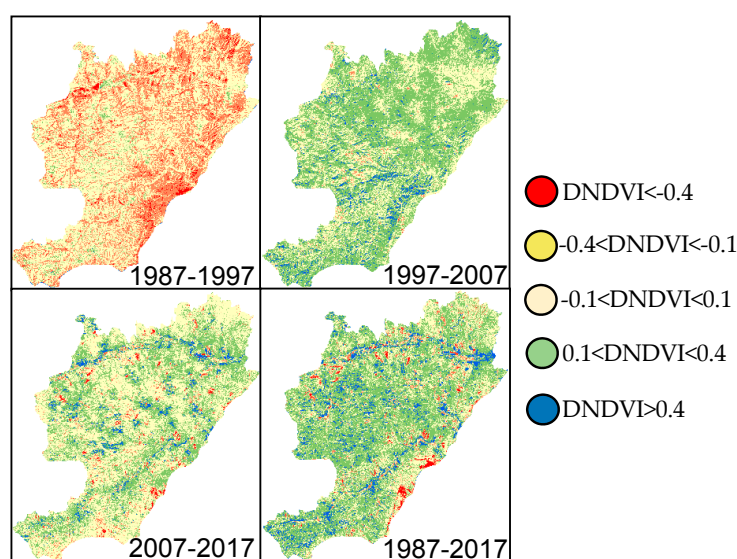**Figure 10.** The distribution of NDVI in 1987, 1997, 2007, and 2017.

Figure 11. The distribution of difference-NDVI (DNDVI) which was calculated by the NDVI in 1987, 1997, 2007, and 2017.

We summarized the proportion of DNDVI in each grade and their main two change directions, which were calculated the difference in NDVI between 1987 and 1997, 1997 and 2007, 2007, and 2017, as well as 1987 and 2017, respectively (Table 5). The results showed that in the first 10 years, over 35% of the area presented various decline in NDVI, which was much larger than that in other periods, and only 3.23% of the area showed an increase in NDVI value. The area with a decrease of NDVI can be mainly attributed to the change from forest into low-coverage grassland. Between 1997 and 2007, the NDVI value, 60.88%, in the mining area raised with varied amounts, although the land use in these areas mainly did not change; while the area with a declining trend of NDVI value only accounted for 1.35%, and mostly came from the change from grassland into bare land and buildings. In the next decade, most of the Nanjiao mining area also experienced an increase in NDVI value, which occupied 38.66% of this area and resulted from the decrease of buildings. On the other hand, some buildings and bare land also replaced the area (5.6%) where there used to be mixed forest and low-coverage grassland. Finally, from the perspective of 30 years, 1.34% of the area where the NDVI decreased by more than 0.4 was in the subsidence area, mainly because of the transformation from natural forest to low-coverage grassland; in contrast, low-coverage grassland that had been converted into cultivated forest contributed 4.38% of the area, with an increase of more than 0.4 in NDVI. The remaining areas where NDVI changed mainly involved the inter-transformation between mixed forest and low-coverage grassland, as well as the difference in NDVI between the same land uses.

Table 5. LULC changes based on difference-normalized difference vegetation index (DNDVI) between 1987 and 1997, 1997 and 2007, 2007, and 2017, as well as 1987 and 2017. Note: LC grassland and HC grassland represent low-coverage grassland and high-coverage grassland, respectively.

Year	DNDVI	Proportion (%)	Change Direction (%)
1987–1997	DNDVI <−0.4	2.88	Mixed forest →LC grassland (0.45)
			Natural forest → LC grassland (0.31)
	−0.1 < DNDVI < −0.4	34.78	Mixed forest → LC grassland (9.79)
			LC grassland (3.52)
	−0.1 < DNDVI < 0.1	59.10	LC grassland (18.08)
			Mixed forest → LC grassland (7.58)
	0.1 < DNDVI < 0.4	3.14	LC grassland (1.04)
			Bare land → LC grassland (0.27)
	DNDVI >0.4	0.09	Mixed forest →Natural forest (0.04)
			LC grassland → Shrubs (0.02)
1997–2007	DNDVI <−0.4	0.02	HC grassland → Bare land (0.004)
			LC grassland → Bare land (0.004)
	−0.1< DNDVI < −0.4	1.33	LC grassland → Bare land (0.37)
			LC grassland → Building (0.29)
	−0.1 < DNDVI < 0.1	37.77	LC grassland (17.66)
			Mixed forest (6.40)
	0.1 < DNDVI < 0.4	56.55	LC grassland (14.68)
			LC grassland → Mixed forest (11.68)
	DNDVI >0.4	4.33	Natural forest (1.48)
			Shrub (0.48)
2007–2017	DNDVI <−0.4	0.92	Mixed forest → Building (0.13)
			Mixed forest → Bare land (0.12)
	−0.1< DNDVI < −0.4	4.68	LC grassland → Bare land (0.55)
			Mixed forest → Building (0.45)
	−0.1 < DNDVI < 0.1	55.73	LC grassland (15.10)
			Mixed forest (6.71)
	0.1 < DNDVI < 0.4	35.08	LC grassland (10.45)
			Building → LC grassland (3.61)
	DNDVI >0.4	3.58	Buildings → HC grassland (0.55)
			Buildings →HC grassland (0.51)
1987–2017	DNDVI <−0.4	1.34	Natural forest → LC grassland (0.67)
			Shrubs → Bare land (0.16)
	−0.1< DNDVI < −0.4	4.59	Mixed forest → LC grassland (1.81)
			LC grassland (1.13)
	−0.1 < DNDVI < 0.1	32.49	Mixed forest (14.18)
			LC grass (9.60)
	0.1 < DNDVI < 0.4	53.28	LC grassland → Mixed forest (25.79)
			Mixed forest (17.86)
	DNDVI >0.4	8.29	LC grassland → Cultivated forest (4.38)
			Buildings → Cultivated forest (1.97)

3.3. Relevance Between LULC Changes, Underground Mining, and Reforestation

The partial correlation coefficients between each LULC and coal production, as well as reforestation area, is shown in Table 6. In addition, the fitting curve was also calculated, while the area of natural forest and cultivated forest were selected as examples to be related to coal production and reforestation

areas respectively, due to their close relationship. Buildings and farmland were also chosen to be correlated to coal production and reforestation areas, because they were less influenced by other factors such as climate change. Results showed that coal production was related significantly to most LULC, except cultivated forest, mixed forest, and bare land. Similarly, a significant correlation was also observed between reforestation areas and LULC, in addition to mixed forest and bare land. It also showed that the reforestation project was positively related to cultivated forest, while underground mining had a negative effect on natural forest. The area of farmland and buildings could also be influenced by these two human activities (Figure 12).
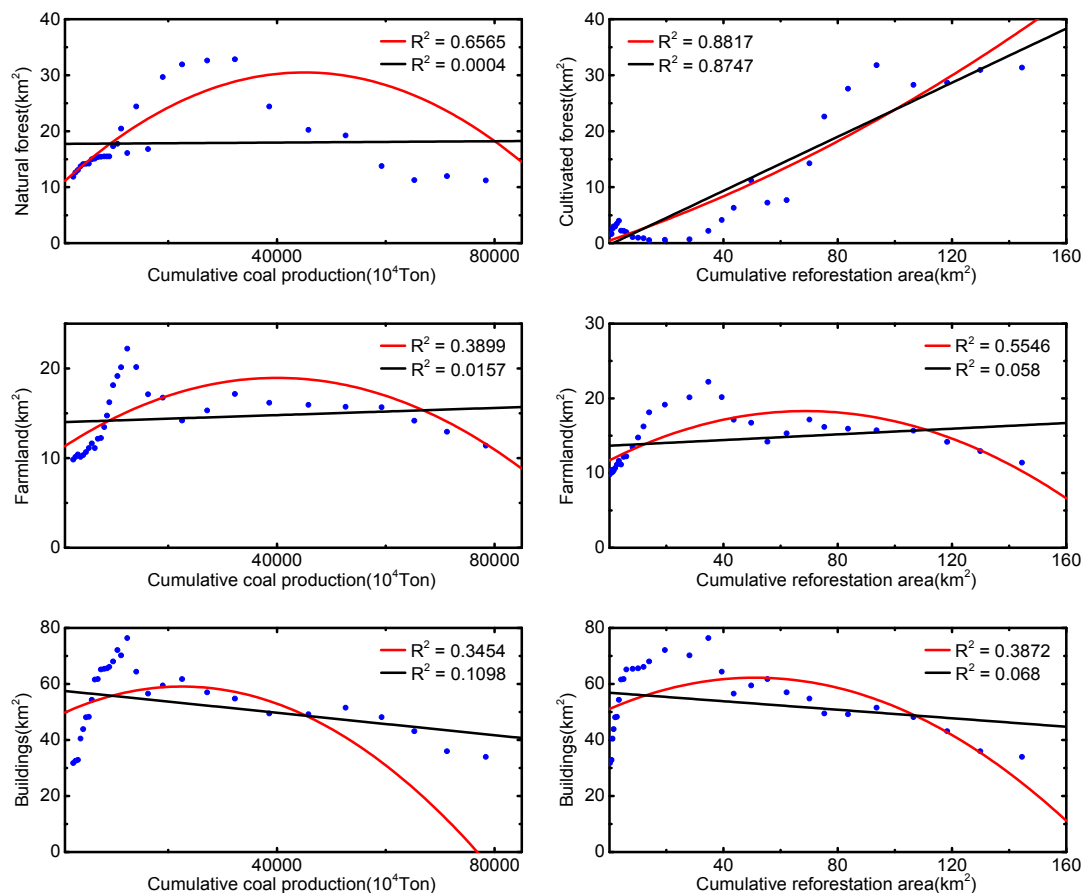
Figure 12. The fitting curve of land use area and coal production, as well as reforestation area. Red line and black line are linear fit curve and non-linear fit curve, respectively.

Table 6. The partial correlation coefficients between LULC and coal production, as well as reforestation area. Note: Photovoltaic panel area was not included due to its short duration. * represents $p < 0.05$. ** represents $p < 0.01$.

LULC	$r_{L_iC \cdot R}$	$r_{L_iR \cdot C}$
Cultivated forest	−0.23	0.66 **
Natural forest	−0.75 **	0.76 **
Buildings	−0.43 *	0.39 *
Farmland	−0.64 *	0.66 **
HC grassland	−0.67 *	0.64 **
Shrubs	0.62 *	−0.48 **
Mixed forest	0.08	−0.14
LC grassland	0.60 **	−0.65 **
Bare land	−0.28	0.22

4. Discussion

4.1. Characteristics of the LULC Change in the Mining Area

The LULC change in the underground mining area was variable and nonlinear. Temporal change results (Figure 7) indicated that the dynamic of LULC in the study area was fluctuant rather than gradual, which showed different development trends in each period; the spatial change (Table 5) revealed that both dramatically and slightly changed areas were distributed in the mining area, and included multiple change directions in LULC. Similar changes trends were also observed in previous research. The area of farmland and water in the Jiawang mining area fluctuated during 25 years, and showed a dramatic change in the first five years [48]. The single LULC pattern in the Bokaro mining area was greatly altered into a complex one after 34 years of coal exploitation, especially when the reclamation was performed to reuse that disturbed area by mining activities [49]. A significant difference in the change of LULC between each part of the Nadowli mining area was observed, showing varying degrees of savanna loss [50]. On the other hand, the nonlinearity of changes in the mining area was also illustrated by some distinctive types of LULC. For example, the buildings in our study area experienced a significant reduction from 2007 to 2017, which was believed as an irreversible LULC in most area. There were numerous driving forces which could interfere with the stable change of LULC, such as continuous underground mining and its accompanied geographic disasters, the change of land use policy, as well as increase of population [51]. Especially in heterogeneous areas, the LULC could be more likely to change under the combined effects of underground mining and other human activities. Thus, it is important to track the dynamic of LULC change in these areas, and understand the underlying driving forces of these changes, which would benefit environmental assessment and land use plan in mining areas.

4.2. Effects of Underground Mining and Reforestation on the Analyzed LULC

Mining and reforestation are considered as two of most intensive human activities that generated land use changes in the underground mining area. The spatial distribution of land use changes illustrated that the areas with dramatic change (DNDVI > 0.4) were likely to be influenced by human activities, which mainly consisted of transformation from buildings and grass land into cultivated forest (Table 5). Furthermore, the correlation between LULC, coal production, and reforestation areas also indicated the effects of underground mining and reforestation projects. In summary, underground mining and reforestation projects could drive LULC change in both the short- and long-term. In the initial period, geological disasters such as surface subsidence and related fissures at the surface caused by underground mining, have destroyed buildings and directly resulted in the death of some vegetation [52,53]. Meanwhile, reforestation projects that occur after the reclamation of mined land will remove the original land use of the mining area and replace it with new LULC in the short term [16]. Over the long-term, underground mining and reforestation projects could alter the LULC in a way that restricts the diversity of the land use: (1) Continuous mining would result in abandonment of many original villages and the relocation of the villagers. In this study area, over 30,000 villagers would move from the Nanjiao mining area due to potential damage of subsidence, and the left villages would be demolished and reclaimed according the land use planning of local government. (2) Some traditional agriculture and aquaculture activities could be abandoned, leading to the disappearance of farmland and grassland. (3) Novel LULC, such as the photovoltaic land in this study, would emerge on the subsided area after reclamation, which could be in a well-planned but single pattern. (4) The ground fissures resulting from mining would also aggravate soil erosion, so that soil erosion would lead to soil degradation and a loss of surface vegetation [54]. (5) Reforestation projects would also limit other human activities, such as agriculture, forestry, and animal husbandry, causing the associated land use to gradually disappear. (6) The reconstruction of land use would improve regional ecosystem regulation and support services, which could promote the succession of native vegetation and result in

the change in LULC. In summary, these effects of underground mining and reforestation projects have highlighted the importance of monitoring the changes of LULC in mining areas.

4.3. Research Limitations and Future Work

A few limitations exist when we tracked the land use change in this area with underground mining and reforestation via continuous Landsat classification, which are: (1) The supervised classification method requires a very large number of training samples, which entails enormous costs in time and effort when accurate training samples are established. (2) other factors may influence the results. Our study only discussed the effects of underground mining and reforestation projects on the LULC, while the correlation between climatic factors, other human activities, and other LULC changes were not well demonstrated. Moreover, topography could also influence the accuracy of classification in heterogeneous areas, and the effect of topography information on different LULC classification approaches requires investigation at multiple scales in future research. (3) Impacts caused by underground mining and reforestation should be quantified. Some direct or potential effects of underground mining and reforestation projects, such as changes to groundwater near the mining face and the distribution of ground fissures, were not analyzed and quantified in the present study.

In the near future, we plan to conduct further research in this area. First, high-resolution images could be combined with radar data to improve the accuracy of the Landsat image classification results. Google Earth imagery provides no-cost imagery with ultra-high definition in the red, green, and blue spectral bands, which could provide crucial information that could be used to identify and extract the shapes of surface objects. Radar data is believed to have potential usefulness in LULC classification, because of its ability to penetrate trees, shrubs, and herbaceous vegetation [55,56]. Therefore, multivariate remote sensing data could be used to improve the accuracy of training samples and thus the accuracy of classification results. In addition, the effects of climate change and other human factors need to be removed from complex LULC changes to better quantify the effects of underground mining and reforestation projects. Comparing the mining and non-mining areas that have similar climates, initial vegetation, and human activity could be an effective way to eliminate the effects of other factors on LULC changes. Moreover, we also plan for a detailed investigation of the geological conditions, groundwater levels, and surface soil changes in the mining area to qualify the effects of underground mining; this would allow us to investigate the potential damage caused by mining activities to surface vegetation and explain the mechanisms of LULC changes in the mining area.

5. Conclusions

The objective of this research was to monitor LULC-scale changes in a heterogeneous area with continuous underground mining and reforestation projects. This was done with continuous Landsat images via random forest classifier, which could provide critical information for an environmental assessment and ecological restoration efforts. We also discussed the correlation between LULC changes and both underground mining and reforestation projects.

In this research, we monitored the LULC change in the Nanjiao mining area between 1987 and 2017. Continuous Landsat classification was demonstrated to have excellent performance in tracking the dynamics of the LULC, which could effectively minimize errors and eliminate misleading trends caused by large time gaps. A random forest classifier was also applied, which showed an average of 84.01% overall accuracy, achieving excellent performance in this area with strong heterogeneity and multi-factor disturbances. In addition, we also identified correlations between LULC areas and coal production, as well as the reforestation area. After an increase in the reforestation area that has occurred since 2004, the areas of cultivated forest increased at a stable rate, while the spatial extent of natural forest declined significantly after 2007 when coal production increased dramatically. Buildings and farmland were likely to be related to both coal production and reforestation areas. This could indicate the relevance of a connection between LULC changes and underground mining, as well as reforestation projects.

The results show that continuous Landsat data can be an important resource when detecting changes in a LULC. This research could enhance our understanding of LULC changes in an area with continuous underground mining and reforestation, and provide a reference that can be used to illustrate the drivers of LULC change. The acquired information could be applied to land use planning, ecological restoration strategies, and the development of environmentally sound management policies in a mining area.

References

1. Ales, R.F.; Martin, A.; Ortega, F.; Ales, E.E. Recent changes in landscape structure and function in a mediterranean region of SW Spain (1950–1984). *Landsc. Ecol.* **1992**, *7*, 3–18. [CrossRef]
2. Kareiva, P.; Wennergren, U. Connecting landscape patterns to ecosystem and population processes. *Nature* **1995**, *373*, 299–302. [CrossRef]
3. Tscharntke, T.; Klein, A.M.; Kruess, A.; Steffan-Dewenter, I.; Thies, C. Landscape perspectives on agricultural intensification and biodiversity-ecosystem service management. *Ecol. Lett.* **2005**, *8*, 857–874. [CrossRef]
4. Xiao, W.; Fu, Y.; Wang, T.; Lv, X. Effects of land use transitions due to underground coal mining on ecosystem services in high groundwater table areas: A case study in the Yanzhou coalfield. *Land Use Policy* **2018**, *71*, 213–221. [CrossRef]
5. Liu, S.; Wang, T. Aeolian processes and landscape change under human disturbances on the Sonid grassland of inner Mongolian Plateau, northern China. *Environ. Earth Sci.* **2014**, *71*, 2399–2407. [CrossRef]
6. Wang, Y.Q.; Zhang, X.S. A dynamic modeling approach to simulating socioeconomic effects on landscape changes. *Ecol. Model.* **2001**, *140*, 141–162. [CrossRef]
7. D'Almeida, C.; Vörösmarty, C.J.; Hurtt, G.C.; Marengo, J.A.; Dingman, S.L.; Keim, B.D. The effects of deforestation on the hydrological cycle in Amazonia: A review on scale and resolution. *Int. J. Climatol.* **2010**, *27*, 633–647. [CrossRef]
8. Li, J.; Zipper, C.E.; Donovan, P.F.; Wynne, R.H.; Oliphant, A.J. Reconstructing disturbance history for an intensively mined region by time-series analysis of Landsat imagery. *Environ. Monit. Assess.* **2015**, *187*, 557. [CrossRef] [PubMed]
9. Skalos, J.; Kasparova, I. Landscape memory and landscape change in relation to mining. *Ecol. Eng.* **2012**, *43*, 60–69. [CrossRef]
10. Lei, K.; Pan, H.; Lin, C. A landscape approach towards ecological restoration and sustainable development of mining areas. *Ecol. Eng.* **2016**, *90*, 320–325. [CrossRef]
11. Wang, J.; Wang, P.; Qin, Q.; Wang, H. The effects of land subsidence and rehabilitation on soil hydraulic properties in a mining area in the Loess Plateau of China. *Catena* **2017**, *159*, 51–59. [CrossRef]
12. He, Y.; He, X.; Liu, Z.; Zhao, S.; Bao, L.; Li, Q.; Yan, L. Coal mine subsidence has limited impact on plant assemblages in an arid and semi-arid region of northwestern China. *Écoscience* **2017**, *24*, 91–103. [CrossRef]
13. Hu, Z.; Xu, X.; Zhao, Y. Dynamic monitoring of land subsidence in mining area from multi-source remote-sensing data—A case study at Yanzhou, China. *Int. J. Remote Sens.* **2012**, *33*, 5528–5545. [CrossRef]
14. Zipper, C.E.; Burger, J.A.; Skousen, J.G.; Angel, P.N.; Barton, C.D.; Davis, V.; Franklin, J.A. Restoring Forests and Associated Ecosystem Services on Appalachian Coal Surface Mines. *Environ. Manag.* **2011**, *47*, 751–765. [CrossRef]

15. Román-Dañobeytia, F.; Huayllani, M.; Michi, A.; Ibarra, F.; Loayza-Muro, R.; Vázquez, T.; Rodríguez, L.; García, M. Reforestation with four native tree species after abandoned gold mining in the Peruvian Amazon. *Ecol. Eng.* **2015**, *85*, 39–46. [CrossRef]

16. Evans, D.M.; Zipper, C.E.; Burger, J.A.; Strahm, B.D.; Villamagna, A.M. Reforestation practice for enhancement of ecosystem services on a compacted surface mine: Path toward ecosystem recovery. *Ecol. Eng.* **2013**, *51*, 16–23. [CrossRef]

17. Jorgenson, M.T.; Frost, G.V.; Dissing, D. Drivers of Landscape Changes in Coastal Ecosystems on the Yukon-Kuskokwim Delta, Alaska. *Remote Sens.* **2018**, *10*, 1280. [CrossRef]

18. Jorgenson, J.C.; Jorgenson, M.T.; Boldenow, M.L.; Orndahl, K.M. Landscape Change Detected over a Half Century in the Arctic National Wildlife Refuge Using High-Resolution Aerial Imagery. *Remote Sens.* **2018**, *10*, 1305. [CrossRef]

19. Curatola Fernández, G.; Obermeier, W.; Gerique, A.; López Sandoval, M.; Lehnert, L.; Thies, B.; Bendix, J. Land Cover Change in the Andes of Southern Ecuador—Patterns and Drivers. *Remote Sens.* **2015**, *7*, 2509–2542. [CrossRef]

20. DeWitt, J.D.; Chirico, P.G.; Bergstresser, S.E.; Warner, T.A. Multi-scale 46-year remote sensing change detection of diamond mining and land cover in a conflict and post-conflict setting. *Remote Sens. Appl. Soc. Environ.* **2017**, *8*, 126–139. [CrossRef]

21. Soulard, C.E.; Acevedo, W.; Stehman, S.V.; Parker, O.P. Mapping Extent and Change in Surface Mines Within the United States for 2001 to 2006. *Land Degrad. Dev.* **2016**, *27*, 248–257. [CrossRef]

22. Du, P.; Yuan, L.; Xia, J.; He, J. Fusion and classification of Beijing-1 small satellite remote sensing image for land cover monitoring in mining area. *Chin. Geogr. Sci.* **2011**, *21*, 656–665. [CrossRef]

23. De Lucia Lobo, F.; Souza-Filho, P.W.M.; De Moraes Novo, E.M.L.; Carlos, F.M.; Barbosa, C.C.F. Mapping Mining Areas in the Brazilian Amazon Using MSI/Sentinel-2 Imagery (2017). *Remote Sens.* **2018**, *10*, 1178. [CrossRef]

24. Raczko, E.; Zagajewski, B. Comparison of support vector machine, random forest and neural network classifiers for tree species classification on airborne hyperspectral APEX images. *Eur. J. Remote Sens.* **2017**, *50*, 144–154. [CrossRef]

25. Pal, M. Random forest classifier for remote sensing classification. *Int. J. Remote Sens.* **2007**, *26*, 217–222. [CrossRef]

26. Berhane, T.M.; Lane, C.R.; Wu, Q.; Autrey, B.C.; Anenkhonov, O.A.; Chepinoga, V.V.; Liu, H. Decision-Tree, Rule-Based, and Random Forest Classification of High-Resolution Multispectral Imagery for Wetland Mapping and Inventory. *Remote Sens.* **2018**, *10*, 580. [CrossRef] [PubMed]

27. Cui, Y.; Li, L.; Chen, L.; Zhang, Y.; Cheng, L.; Zhou, X.; Yang, X. Land-Use Carbon Emissions Estimation for the Yangtze River Delta Urban Agglomeration Using 1994–2016 Landsat Image Data. *Remote Sens.* **2018**, *10*, 1334. [CrossRef]

28. Mohamed, H.; Nadaoka, K.; Nakamura, T. Assessment of Machine Learning Algorithms for Automatic Benthic Cover Monitoring and Mapping Using Towed Underwater Video Camera and High-Resolution Satellite Images. *Remote Sens.* **2018**, *10*, 773. [CrossRef]

29. Pei, W.; Yao, S.; Knight, J.F.; Dong, S.; Pelletier, K.; Rampi, L.P.; Wang, Y.; Klassen, J. Mapping and detection of land use change in a coal mining area using object-based image analysis. *Environ. Earth Sci.* **2017**, *76*. [CrossRef]

30. Townsend, P.A.; Helmers, D.P.; Kingdon, C.C.; McNeil, B.E.; de Beurs, K.M.; Eshleman, K.N. Changes in the extent of surface mining and reclamation in the Central Appalachians detected using a 1976–2006 Landsat time series. *Remote Sens. Environ.* **2009**, *113*, 62–72. [CrossRef]

31. Petropoulos, G.P.; Partsinevelos, P.; Mitraka, Z. Change detection of surface mining activity and reclamation based on a machine learning approach of multi-temporal Landsat TM imagery. *Geocarto Int.* **2013**, *28*, 323–342. [CrossRef]

32. Ji, L.; Gong, P.; Geng, X.; Zhao, Y. Improving the Accuracy of the Water Surface Cover Type in the 30 m FROM-GLC Product. *Remote Sens.* **2015**, *7*, 13507–13527. [CrossRef]

33. Brovelli, M.; Molinari, M.; Hussein, E.; Chen, J.; Li, R. The First Comprehensive Accuracy Assessment of GlobeLand30 at a National Level: Methodology and Results. *Remote Sens.* **2015**, *7*, 4191–4212. [CrossRef]

34. Kennedy, R.E.; Yang, Z.; Cohen, W.B. Detecting trends in forest disturbance and recovery using yearly Landsat time series: 1. LandTrendr—Temporal segmentation algorithms. *Remote Sens. Environ.* **2010**, *114*, 2897–2910. [CrossRef]

35. Yang, Y.; Erskine, P.D.; Lechner, A.M.; Mulligan, D.; Zhang, S.; Wang, Z. Detecting the dynamics of vegetation disturbance and recovery in surface mining area via Landsat imagery and LandTrendr algorithm. *J. Clean. Prod.* **2018**, *178*, 353–362. [CrossRef]

36. Liu, S.; Wei, X.; Li, D.; Lu, D. Examining Forest Disturbance and Recovery in the Subtropical Forest Region of Zhejiang Province Using Landsat Time-Series Data. *Remote Sens.* **2017**, *9*, 479. [CrossRef]

37. Garrigues, S.; Allard, D.; Baret, F.; Weiss, M. Influence of landscape spatial heterogeneity on the non-linear estimation of leaf area index from moderate spatial resolution remote sensing data. *Remote Sens. Environ.* **2006**, *105*, 286–298. [CrossRef]

38. *General Planning of Mineral Resources in the Southern Suburb of Datong City*; Government, Department of Safety and Professional Services: Datong, China, 2012.

39. Yang, X.; Xu, B.; Jin, Y.; Qin, Z.; Ma, H.; Li, J.; Zhao, F.; Chen, S.; Zhu, X. Remote sensing monitoring of grassland vegetation growth in the Beijing-Tianjin sandstorm source project area from 2000 to 2010. *Ecol. Indic.* **2015**, *51*, 244–251. [CrossRef]

40. Wang, X.M.; Zhang, C.X.; Hasi, E.; Dong, Z.B. Has the Three Norths Forest Shelterbelt Program solved the desertification and dust storm problems in arid and semiarid China? *J. Arid Environ.* **2010**, *74*, 13–22. [CrossRef]

41. Chander, G.; Markham, B.L.; Helder, D.L. Summary of current radiometric calibration coefficients for Landsat MSS, TM, ETM+, and EO-1 ALI sensors. *Remote Sens. Environ.* **2009**, *113*, 893–903. [CrossRef]

42. Raval, S.; Shamsoddini, A. A monitoring framework for land use around kaolin mining areas through Landsat TM images. *Earth Sci. Inform.* **2014**, *7*, 153–163. [CrossRef]

43. Chen, J.; Jönsson, P.; Tamura, M.; Gu, Z.; Matsushita, B.; Eklundh, L. A simple method for reconstructing a high-quality NDVI time-series data set based on the Savitzky—Golay filter. *Remote Sens. Environ.* **2004**, *91*, 332–344. [CrossRef]

44. Savitzky, A.; Golay, M.J.E. Smoothing and differentiation of data by simplified least squares procedures. *Anal. Chem.* **1967**, *36*, 1627–1639. [CrossRef]

45. Stehman, S.V. Model-assisted estimation as a unifying framework for estimating the area of land cover and land-cover change from remote sensing. *Remote Sens. Environ.* **2009**, *113*, 2455–2462. [CrossRef]

46. Vázquez-Jiménez, R.; Ramos-Bernal, R.N.; Romero-Calcerrada, R.; Arrogante-Funes, P.; Tizapa, S.S.; Novillo, C.J. Thresholding Algorithm Optimization for Change Detection to Satellite Imagery. In *Colorimetry and Image Processing*; Travieso-González, C.M., Ed.; InTech: London, UK, 2018.

47. Lu, D.; Li, G.; Moran, E. Current situation and needs of change detection techniques. *Int. J. Image Data Fusion* **2014**, *5*, 13–38. [CrossRef]

48. Bian, Z.; Lu, Q. Ecological effects analysis of land use change in coal mining area based on ecosystem service valuing: A case study in Jiawang. *Environ. Earth Sci.* **2012**, *68*, 1619–1630. [CrossRef]

49. Malaviya, S.; Munsi, M.; Oinam, G.; Joshi, P.K. Landscape approach for quantifying land use land cover change (1972–2006) and habitat diversity in a mining area in Central India (Bokaro, Jharkhand). *Environ. Monit. Assess.* **2010**, *170*, 215–229. [CrossRef]

50. Basommi, L.P.; Guan, Q.; Cheng, D.; Singh, S.K. Dynamics of land use change in a mining area: A case study of Nadowli District, Ghana. *J. Mt. Sci.* **2016**, *13*, 633–642. [CrossRef]

51. Liu, C.; Ma, X. Analysis to driving forces of land use change in Lu'an mining area. *Trans. Nonferr. Met. Soc. China* **2011**, *21*, s727–s732. [CrossRef]

52. Yilmaz, I.; Marschalko, M. A leaning historical monument formed by underground mining effect: An example from Czech Republic. *Eng. Geol.* **2012**, *133*, 43–48. [CrossRef]

53. Dong, S.C.; Samsonov, S.; Yin, H.W.; Yao, S.P.; Xu, C. Spatio-temporal analysis of ground subsidence due to underground coal mining in Huainan coalfield, China. *Environ. Earth Sci.* **2015**, *73*, 5523–5534. [CrossRef]

54. Lechner, A.M.; Baumgartl, T.; Matthew, P.; Glenn, V. The Impact of Underground Longwall Mining on Prime Agricultural Land: A Review and Research Agenda. *Land Degrad. Dev.* **2016**, *27*, 1650–1663. [CrossRef]

55. Yang, Z.; Dong, J.; Qin, Y.; Ni, W.; Zhao, G.; Chen, W.; Chen, B.; Kou, W.; Wang, J.; Xiao, X. Integrated Analyses of PALSAR and Landsat Imagery Reveal More Agroforests in a Typical Agricultural Production Region, North China Plain. *Remote Sens.* **2018**, *10*, 1323. [CrossRef]

56. De Alban, J.; Connette, G.; Oswald, P.; Webb, E. Combined Landsat and L-Band SAR Data Improves Land Cover Classification and Change Detection in Dynamic Tropical Landscapes. *Remote Sens.* **2018**, *10*, 306. [CrossRef]